Cardiovascular Research (2016) **112**, 645–655
doi:10.1093/cvr/cvw214

Magnetic resonance imaging of infarct-induced canonical wingless/integrated (Wnt)/β-catenin/T-cell factor pathway activation, *in vivo*

Marco Matteucci[1], Valentina Casieri[1], Khatia Gabisonia[1], Giovanni Donato Aquaro[2], Silvia Agostini[1], Giuseppe Pollio[3], Daniela Diamanti[3], Marco Rossi[3], Massimiliano Travagli[3], Valentina Porcari[3], Fabio A. Recchia[1,4†], and Vincenzo Lionetti[1,2*†]

[1]Laboratory of Medical Science, Institute of Life Sciences, Scuola Superiore Sant'Anna, Via G. Moruzzi, 1, 56124 Pisa, Italy; [2]Fondazione Toscana 'G. Monasterio', 56124 Pisa, Italy; [3]Siena Biotech Medicine Research Centre, 53100 Siena, Italy; and [4]Cardiovascular Research Center, Lewis Katz School of Medicine, Temple University, 19140 Philadelphia, PA, USA

Received 3 February 2016; revised 6 September 2016; accepted 15 September 2016; online publish-ahead-of-print 26 September 2016

Time of primary review: 43 days

Aims Combined magnetic resonance imaging (MRI) of molecular and morpho-functional changes might prove highly valuable for the elucidation of pathological processes involved in the development of cardiac diseases. Our aim was to test a novel MRI reporter gene for *in vivo* assessment of the canonical Wnt/β-catenin/TCF pathway activation, an important regulator of post-ischaemic cardiac remodelling.

Methods and results We designed and developed a chimeric construct encoding for both of iron-binding human ferritin heavy chain (hFTH) controlled by the β-catenin-responsive TCF/lymphoid-enhancer binding factor (Lef) promoter and constitutively expressed green fluorescent protein (GFP). It was carried by adeno-associated virus serotype 9 (rAAV9) vectors and delivered to the peri-infarct myocardium of rats subjected to coronary ligation ($n = 11$). By 1.5 T MRI and a multiecho T2* gradient echo sequence, we detected iron accumulation only in the border zone of the transduced infarcted hearts. In the same cardiac area, post-mortem histological analysis confirmed the co-existence of iron accumulation and GFP. The iron signal was absent when rats ($n = 6$) were chronically treated with SEN195 (10 mg/kg/day), a small-molecular inhibitor of β-catenin/TCF-dependent gene transcription. Canonical Wnt pathway inhibition attenuated the post-ischaemic remodelling process, as demonstrated by the significant preservation of cardiac function, the 42 ± 1% increase of peri-infarct arteriolar density and 43 ± 3% reduction in infarct scar size compared with untreated animals.

Conclusions The TCF/Lef promoter-hFTH construct is a novel and reliable MRI reporter gene for *in vivo* detection of the canonical Wnt/β-catenin/TCF activation state in response to cardiac injury and therapeutic interventions.

Keywords Myocardial infarction • Ferritin • Reporter gene • MRI • Wnt

1. Introduction

The iron-binding human ferritin heavy chain (hFTH) can be utilized as a reporter gene for *in vivo* magnetic resonance imaging (MRI), as previously shown by other authors[1–5] and by us[6]: hFTH overexpression causes non-toxic intracellular iron accumulation that, in turn, produces measurable areas of relative hypointensity in T2- and T2*-weighted images. Iron enrichment is clearly identifiable by MRI in rodent hearts expressing hFTH[7] or implanted with stem cells transduced with this reporter gene.[5–6] If controlled by promoters sensitive to specific intracellular signals, hFTH might therefore prove highly valuable for combined MRI assessments, *in vivo*, of molecular and morpho-functional changes correlated with the evolution of cardiac pathological processes.

A seemingly major regulator of post-ischaemic cardiac remodelling is the canonical wingless/integrated (Wnt)/β-catenin pathway.[8] Wnt is a secreted polypeptide factor that inhibits glycogen synthase kinase-3β in a

* Corresponding author. Tel: +39 050 315 3534; fax: +39 050 315 2166, E-mail: v.lionetti@sssup.it

† The last two authors contributed equally to the study.

receptor-dependent manner and increases the cytoplasmic levels of non-phosphorylated β-catenin, which translocates into the nucleus and activates gene transcription by interacting with the T-cell factor (TCF)/lymphoid-enhancer binding factor (TCF/Lef) promoter.[8,9] In the absence of Wnt, phosphorylation marks β-catenin for proteasomal degradation.[10] In mice, β-catenin down-regulation attenuates post-ischaemic cardiac remodelling, indicating a detrimental role of the canonical Wnt/β-catenin pathway in this pathological condition.[11–14] However, other reports lead to opposite conclusions.[15–18] Therefore, the elucidation of this controversial pathophysiological aspect might benefit from a technology that permits to correlate, *in vivo*, cardiac morpho-functional changes with the activation state of the canonical Wnt/β-catenin pathway. In this study, we tested a novel TCF/Lef promoter-hFTH construct designed as an MRI reporter

Gene specifically induced by β-catenin and therefore responsive to the Wnt/β-catenin pathway activation after myocardial infarction (MI). TCF/Lef promoter-hFTH was delivered to rat hearts via adeno-associated viral (AAV) vectors. The specificity of this MRI reporter gene was further tested by treating the rats with SEN461 analogue, a Wnt inhibitor/Axin stabilizer leading to β-catenin down-regulation, previously developed and validated by us.[19–21]

2. Methods

2.1 Construction of the reporter gene and encapsidation in rAAV serotype 9 vectors

The hFTH cDNA was amplified by PCR from pCMV6-Entry-hFTH-Myc-DDk-tag plasmid (OriGene Technologies, Rockville, MD, USA). The cloning strategy utilized an intermediate construct to shuttle the correct sequences to the final AAV-based plasmid. This intermediate, the pCDH-EF1-TCF/Lef-hFTH-BGH-PGK-copGFP-T2A-puro, was then used to transfer the whole expression cassette containing the hFTH under control of the Wnt responsive element TCF/Lef, and the copGFP, under the constitutive PGK promoter, into the *Eco*RI–*Xho*I sites of the AAV-Basic2 plasmid (Vector Biolabs Inc., Philadelphia, PA, USA). The sequences of all plasmids were verified through full sequencing process (Eurofins Genomics-MWG Operon, Ebersberg, Germany). Primers employed for cloning and sequencing were purchased from SIGMA-ALDRICH (Milan, Italy). Kit for mini-prep and maxi-prep purification and for gel extraction was purchased from QIAGEN (Venlo, Holland). To obtain rAAV serotype nine particles (rAAV9) at the high titre and high purity grade suitable for *in vivo* use, and for the scaling up of the viral production, our final reporter construct was shipped to Vector Biolabs Inc. Titres of rAAV9 particles were expressed as number of genome copies (GC) per millilitre.

2.2 In vitro validation of the reporter plasmid function

Human embryonic kidney (HEK)-293 cells were transfected with pAAV-Basic-TCF/Lef-hFTH-BGH-PGK-copGFP-T2A-puro using JetPrime transfection reagent (Polyplus-transfection, France), according to manufacturer's instructions. Cell transfection efficiency was assessed by flow cytometry. First, basal and inducible levels of expression of the final reporter plasmid were tested *in vitro* by assessing mRNA levels for both hFTH and copGFP through retro-transcribed quantitative PCR (RT-qPCR). Culture media containing Wnt3a (Wnt3a-CM) was harvested from murine fibroblasts secreting Wnt3a (L-cells, ATCC CRL-2648), according to the ATCC protocol, and was used to induce responsiveness of canonical Wnt/-catenin pathway. Control medium (L-CM) and Wnt3a-CM were prepared as previously described.[22] Non-transfected (HEK)-293 cells represented the negative control. After 24 h of treatment with Wnt3a-CM or L-CM, RT-qPCR was performed on retro-transcribed cDNA obtained from the total RNA extracted from the above-mentioned HEK293-treated cells, employing a standard RNAeasy Plus mini kit (QIAGEN GmbH, Hilden, Germany). Purified RNA was quantified by Nanodrop ND-1000 Spectrophotometer (Agilent Technologies, Palo Alto, CA, USA) and 1 μg of RNA was used to synthesize cDNA by QuantiTect Reverse Transcription kit (QIAGEN GmbH). RT–qPCRs on cDNA samples were performed using a CFX96 Real Time System/C1000 Thermal cycler (Bio-Rad, Hercules, CA, USA) with iQ™ SYBR Green master mix 2X (Bio-Rad) with primers that specifically amplified the hFTH (for-TGAGCAGGTGAAAGCCATC; rev-GATATTC CGCCAAGCCAGAT), copGFP (for-CCAACAAGATGAAGAGCACC AA; rev-GCAGGAAGGGGTTCTCGTA), or control genes (ACT-for TTAGTTGCGTTACACCCTTTCTTG; ACT-rev GCTGTCACCTTCA CCGTTCC; RPL13a-for CCTGGAGGAGAAGAGGAAAGAGA; RPL13a-rev TTGAGGACCTCTGTGTATTTGTCAA; YWHAZ-for ACTTTTGG TACATTGTGGCTTCAA; YWHAZ-rev CCGCCAGGACAAACCAGT AT). RT–qPCR expression data were normalized on expression of Hs-ACTb, Hs-YWHAZ, and Hs-RPL13a, as described by Vandesompele *et al.*[23] The relative quantification was calculated by ΔΔCt method using a specific manager software for real-time data analysis (iQ5 Software; Bio-Rad). The normalized expression levels of the target gene [hFTH or green fluorescent protein (GFP)] in control condition were expressed as 1. The ratio between this value and the normalized expression levels of hFTH or GFP in the treated samples was reported as normalized fold change. The qPCR analysis was performed in triplicate. In additional experiments, hFTH and copGFP protein expression in transfected (HEK)-293 cells was evaluated by western blot after 24 h incubation with increasing doses (50, 100, and 200 ng/mL) of human recombinant Wnt3A protein (R&D Systems Inc., MN, USA; dissolved in sterile water and stored at −20 °C). Human recombinant Wnt3A protein was added to cell culture medium 24 h after cell transfection.[24,25] Similarly, the reporter gene expression upon treatment with 200 ng/mL of Wnt3A[25] was evaluated in the presence or absence of increasing doses (5, 10, and 50 μM for 24 h) of SEN0109195 (SEN195; Siena Biotech, Siena, Italy), a new Wnt inhibitor/Axin stabilizer and analogue of SEN461.[19–21]

2.3 Western blotting analysis

Equal amounts of protein extracted with radioimmunoprecipitation assay (RIPA) buffer from cell pellets were processed for western blotting assay. Membranes were blocked with 5% milk in TBS/Tween (0.01%) at room temperature for 1 h, and then incubated with the following primary antibodies: anti-hFTH (Santa Cruz Biotechnology, CA, USA, 1:1000 dilution), anti-GFP (AbCam, Cambridge, UK, 1:1000 dilution), and anti-GAPDH (Thermo Fisher Scientific, MA, USA, 1:5000 dilution).

Membranes were then incubated with appropriate horseradish peroxidase-conjugated anti-rabbit or anti-mouse secondary antibodies (Abcam). Specific protein bands were detected using Pierce ECL western blotting substrate (Thermo Fisher Scientific). Protein bands were quantified using ImageJ software. GFP expression was normalized over GAPDH. hFTH expression was normalized over GFP expression. All western blot experiments were performed in triplicate.

2.4 Surgery and experimental protocol

Non-reperfused MI was induced as previously described by us.[6,26–30] Briefly, the left anterior descending coronary artery was ligated near its origin in male adult Wistar rats (body weight 350–400 g) anaesthetized with a

cocktail of tiletamine and zolazepam (Zoletil 100, Virbac, France; dosage 40 mg/kg i.p.), intubated, and ventilated. The viable myocardium bordering the left ventricular (LV) pale ischaemic area was immediately injected at two different sites with a total of 100 µL of one of the following solutions: PBS (MI + PBS, $n = 10$) and 1.1×10^{14} GC/mL of rAAV9-pTCF-hFTH-BGH-PGK-copGFP (rAAV9) (MI + rAAV9, $n = 11$). A third experimental group was sham operated and received the same dose of rAAV9 (Sham+ rAAV9, $n = 8$). Finally, two additional MI + rAAV9 groups were treated for 4 weeks with a constant subcutaneous infusion (10 mg/kg/day) of SEN195 dissolved at the concentration of 40 mg/mL in 50% (v/v) PEG400 (MI + rAAV9 + SEN195, $n = 6$), or vehicle (MI + rAAV9 + Vehicle, $n = 10$) via an implanted mini-osmotic pump (Alzet, model 2ML4, Palo Alto, CA, USA). Mini-osmotic pumps were implanted immediately after closing the chest while the animals were still anesthetized. The dose of SEN195 was chosen based on preliminary data of pharmacokinetics in the rat in order to ensure a steady-state blood concentration of 5 M (2.20 mg/L). At 4 weeks, all rats were anaesthetized with Zoletil 100 (40 mg/kg), underwent MRI analysis and were then euthanized with KCl (1–2 mEq/kg, i.v.) to induce diastolic arrest of cardiac activity. MRI scans were not performed for 3 MI + rAAV9 + Vehicle animals. All animal procedures were approved by the Italian Ministry of Health and conducted in conformity with the guidelines from Directive 2010/63/EU of the European Parliament on the protection of animals used for scientific purposes.

2.5 MRI analysis

In vivo MRI assessment of cardiac morphology, function, and iron accumulation was performed using a clinical 1.5 T MR scanner (Signa HDx; General Electric Health Care, Milwaukee, WI, USA) in sedated rats, as previously described by us[6,26] and by others.[3] Cardiac ECG-triggered images were acquired in the same long-axis and short-axis views for both of cine and T2-star (T2*)-weighted gradient-echo sequence (T2*-GRE) with multiple echo times (TE) using parameters previously employed by us.[6] For each view 10 cine-frames were acquired. A total of five short-axis views (to completely scan the ventricular main axis in end-diastole) and four long-axis views (1 vertical, 1 horizontal, and 2

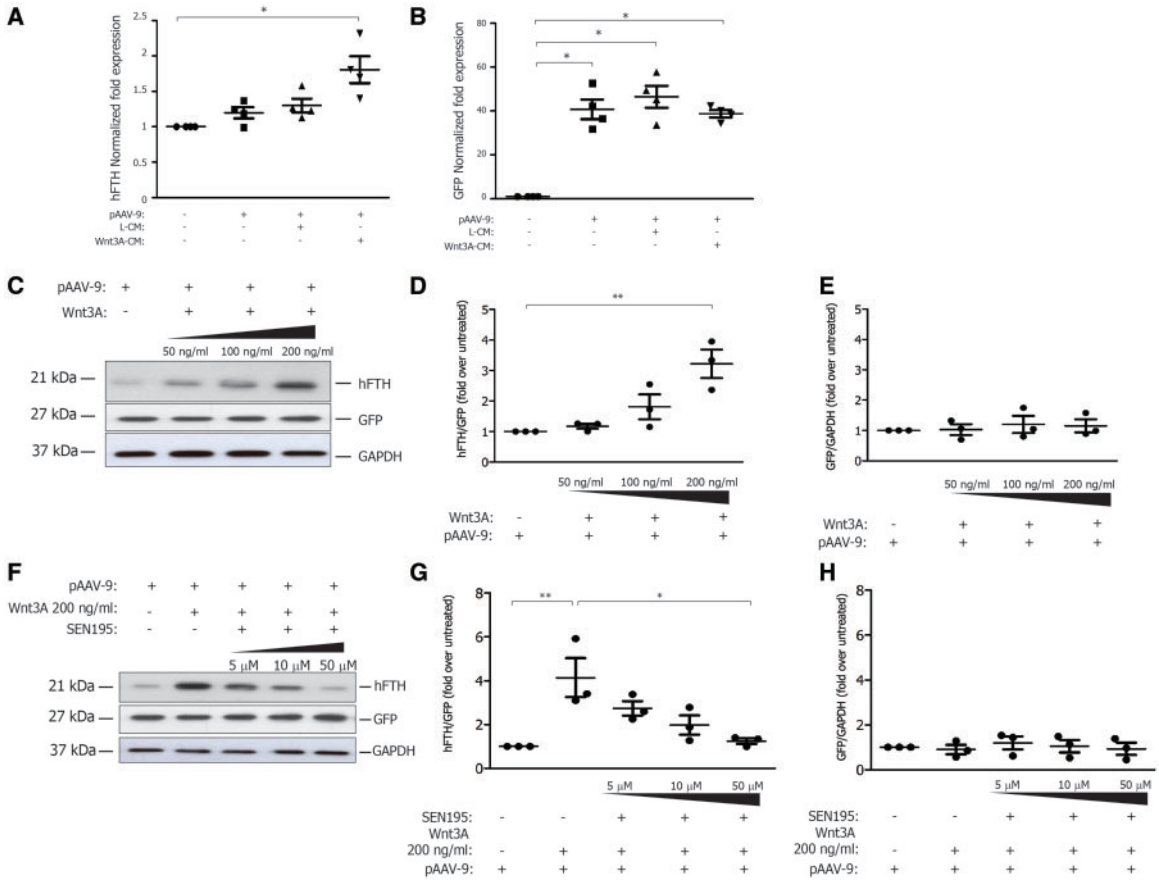

Figure 1 Wnt-dependent induction of hFTH expression is prevented by SEN195, *in vitro*. HEK293 cells wild type (HEK293) and transfected with pAAV-Basic-TCF/Lef-hFTHstop-BGH-PGK-copGFP-T2A-puro (pAAV-9) and cultured with control medium (L-CM) or Wnt3a-conditioned medium (Wnt3a-CM) or human recombinant Wnt3A protein (Wnt3A). (*A*) copGFP gene expression (normalized fold expression) ($n = 4$); (*B*) hFTH gene expression (normalized fold expression) ($n = 4$); (*C*) representative western blot bands for hFTH, GFP, and GAPDH expression at increasing doses of Wnt3A ($n = 3$); (*D*) hFTH/GFP expression (normalized fold expression) ($n = 3$); (*E*) GFP/GAPDH expression (normalized fold expression) ($n = 3$); (*F*) representative western blot bands for hFTH, GFP, and GAPDH expression at increasing doses of SEN195 ($n = 3$); (*G*) hFTH/GFP expression (normalized fold expression) ($n = 3$); (*H*) GFP/GAPDH expression (normalized fold expression) ($n = 3$). One-way ANOVA followed by Bonferroni *post hoc* test (mean ± SEM; in triplicate). $^*P < 0.05$; $^{**}P < 0.01$.

oblique long-axis views) were acquired as previously described by us.[27] LV end-systolic and end-diastolic volume, a marker of cardiac remodelling, and LV ejection fraction were measured and calculated from the cine-images with previously validated software (Mass 6.1; MEDIS, Leiden, The Netherlands). Iron accumulation was detected by measuring myocardial T2*, a transverse relaxation parameter that includes the contribution of magnetic field non-homogeneities. Iron accumulation causes a progressively increasing hypointense that promotes an area reduction in myocardial T2* <20 ms.[6,31] Myocardial T2* was measured in both the LV border zone and the remote zone in long-axis views as previously described.[6] In each region, the calculated decay curve was fitted to the following monoexponential model:

$S = S_0 e^{-TE/T2^*}$,

where S is the signal intensity, $S0$ is the signal value at $TE = 0$, and T2* is the transverse relaxation time constant.

2.6 Histology and immunofluorescence analysis

Hearts were harvested after euthanasia, fixed in 10% buffered formalin, and embedded in paraffin. The LV infarct scar size was measured at each 5 mm-thick transverse section at basal, mid-septal, and apex level using Masson's trichrome-stained images (BIO-OPTICA, Milan, Italy) and by tracing the infarct contours manually with ImageJ software.[6,26–30] At the level of LV mid-septal section, eight serial 5 μm-thick slices were cut and processed for histological, immunofluorescence, and immunohistochemical analysis. Each slice included the entire LV cross section at that level. After being washed in PBS containing 0.1% Tween, the slices were incubated with biotinylated secondary antibodies (Vectastain Elite ABC Kit; Vector Laboratories Inc., USA) and counterstained with haematoxylin. Images were obtained with light microscopy (Olympus BX43) at 10× and 40× original magnification and digitized by a video system (Olympus DP20 camera) interfaced with a computer with dedicated software (CellSens Dimension; Olympus) for morphometric and/or colour analysis.

The density of arterioles in border and remote LV regions was quantified as number of smooth muscle marker α-actin-positive vessels (α-SMA, anti-mouse, 1:100; Santa Cruz Biotechnology). Iron accumulation was detected using Prussian Blue staining (Perls) (BIO-OPTICA) with nuclear-fast red counterstaining. Serial sections were treated with antibodies directed against GFP (anti-rabbit, 1:200; Abcam) and alpha-sarcomeric actin (α-SA; anti-mouse, 1:200; Sigma), a marker of cardiomyocytes, or von Willebrand Factor (vWF; anti-mouse, 1:300, Abcam), an endothelial marker, or α-SMA (anti-mouse, 1:100; Santa Cruz Biotechnology) or neuron-specific nuclear protein (NeuN; anti-guinea pig, 1:100; EMD Millipore). The colocalization of Perls positivity and GFP expression in cardiac cells was assessed by immunofluorescence, as previously described.[6] DyLight 488 goat anti-rabbit (1:200;

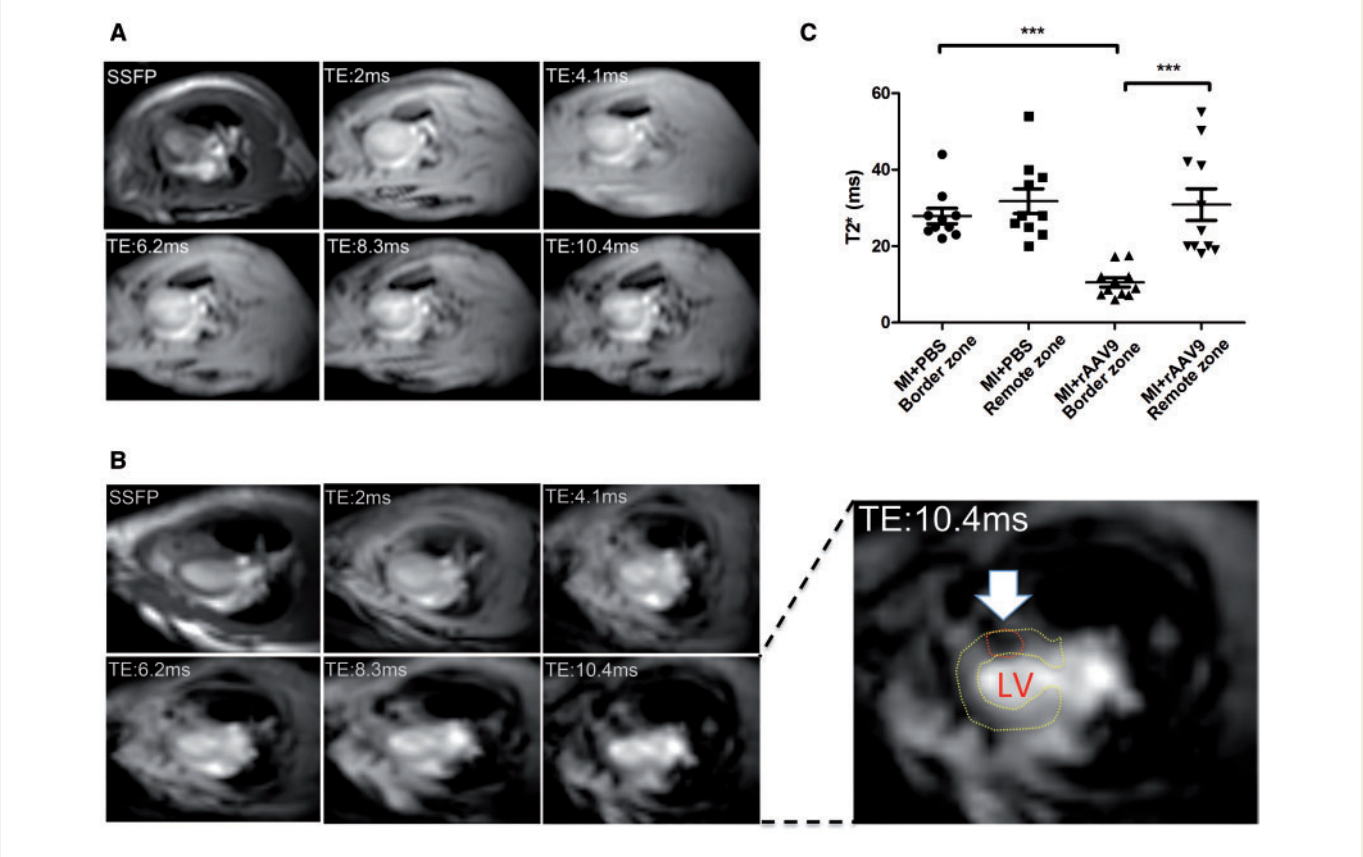

Figure 2 Iron-induced magnetic artefact is detected in rAAV9-transduced infarcted hearts, *in vivo*. MRI detection of iron accumulation at 4 weeks after MI. T2* images at increasing TE in both non-transduced (MI + PBS) (*A*) and transduced (MI + rAAV9) (*B*) infarcted hearts in horizontal long-axis view. The hypointense signal was progressively increasing with TE due to iron accumulation (white arrow and red circle). (*C*; two-way ANOVA with Bonferroni *post hoc* test) Lower T2* values, indicating iron accumulation, were measured in the infarct border zone compared with the remote zone of MI + rAAV9 hearts ($n = 11$). T2* values in the infarct border zone were similar to remote zone of MI + PBS hearts ($n = 10$). SSFP, ECG-triggered steady-state free precession. ***$P < 0.0005$.

Abcam) was used as secondary antibody. No significant fluorescence signal was detectable without secondary antibody. Nuclei were counterstained with 4′,6-Diamidino-2-Phenylindole (DAPI). Fluorescence microscopy was performed with a Leica TCS DMIRE 2 (LCS Lite Software; Leica, Wetzlar, Germany).

2.7 Synthesis of the Wnt signalling inhibitor

SEN0109195 (SEN195) is a Wnt inhibitor/Axin stabilizer characterized by a benzimidazolone structure, whose weight-average molecular weight (Mw) is 440 g/mol. It was developed, validated, and kindly provided by Siena Biotech. Synthetic details for SEN0109195 were reported in the patent application (Pub. No. WO2012/136492). SEN195 action is related to the inhibition of tankyrases (TNK) (IC50 TNK1/TNK2 130 nM/120 nM), an enzyme that leads to selective silencing of TCF-mediated gene transcription by promoting beta-catenin phosphorylation and degradation.[32]

2.8 Statistical analysis

Data are presented as mean ± SEM. One- or two-way analysis of variance (ANOVA) followed by Bonferroni *post hoc* test was used to compare multiple variables. Comparison between two independent groups was performed using the Student's *t*-test. *P*-value <0.05 was set as a threshold for statistical significance. Statistical analysis was performed by employing commercially available software (SPSS for Windows, version 11.1; SPSS, Chicago, IL, USA).

3. Results

3.1 Inducible hFTH and constitutive GFP gene expression

The transfection efficiency in our cells was higher than 90%. As shown in *Figure 1A*, HEK293 cells transfected with pAAV-Basic-TCF/Lef-hFTH-BGH-PGK-copGFP-T2A-puro displayed similar levels of GFP expression under each experimental condition. Conversely, the gene expression of hFTH in HEK293 cells was significantly increased after 24 h of treatment with Wnt3a-CM compared with cells treated with L-CM (*Figure 1B*). As shown in *Figure 1C*, the protein expression of hFTH in transfected cells was increased by Wnt in a concentration-dependent manner (*Figure 1D*), whereas GFP protein expression was unchanged (*Figure 1E*). Finally, the hFTH protein expression induced by Wnt3A treatment was significantly reduced by increasing concentration of SEN195 (*Figure 1G*), whereas GFP expression remained stable. The increased expression of hFTH and the treatment with SEN195 did not affect cell viability and proliferation, as assessed by Trypan Blue staining (not shown).

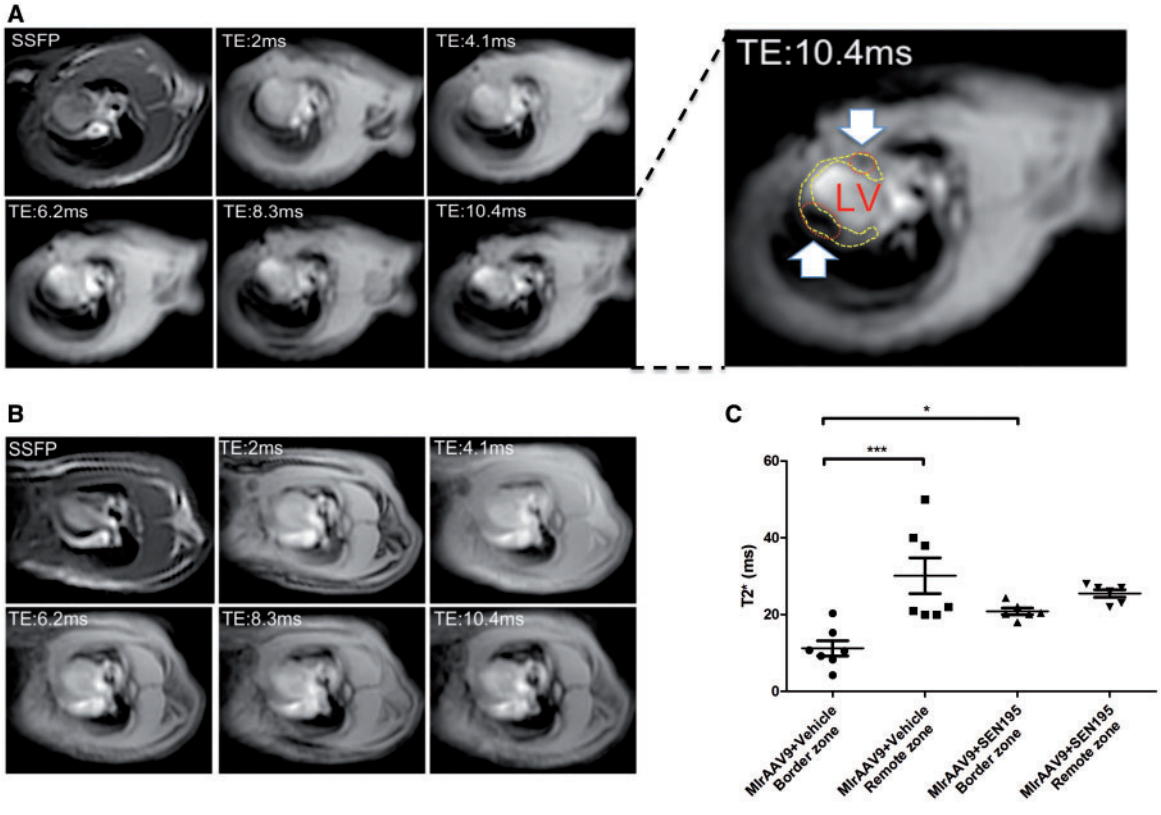

Figure 3 Iron-induced magnetic artefact is undetectable in rAAV9-transduced infarcted hearts treated with Wnt signalling inhibitor, *in vivo*. MRI detection of iron accumulation in transduced infarcted hearts at 4 weeks after SEN195 or Vehicle administration. T2* images at increasing TE in transduced infarcted hearts of rats treated with Vehicle (MI + rAAV9 + Vehicle) (*A*) or SEN195 (MI + rAAV9 + SEN195) (*B*) in horizontal long-axis view. The hypointense area was progressively increasing with TE due to iron accumulation (white arrow and red circle). (*C*; two-way ANOVA with Bonferroni *post hoc* test) Lower T2*values, indicating iron accumulation, were detected in the infarct border zone compared with the remote zone of MI + rAAV9 + Vehicle ($n = 7$). T2*values in the infarct border zone were similar to remote zone of MI + rAAV9 + SEN195 ($n = 6$). SSFP, ECG-triggered steady-state free precession ***$P < 0.001$.

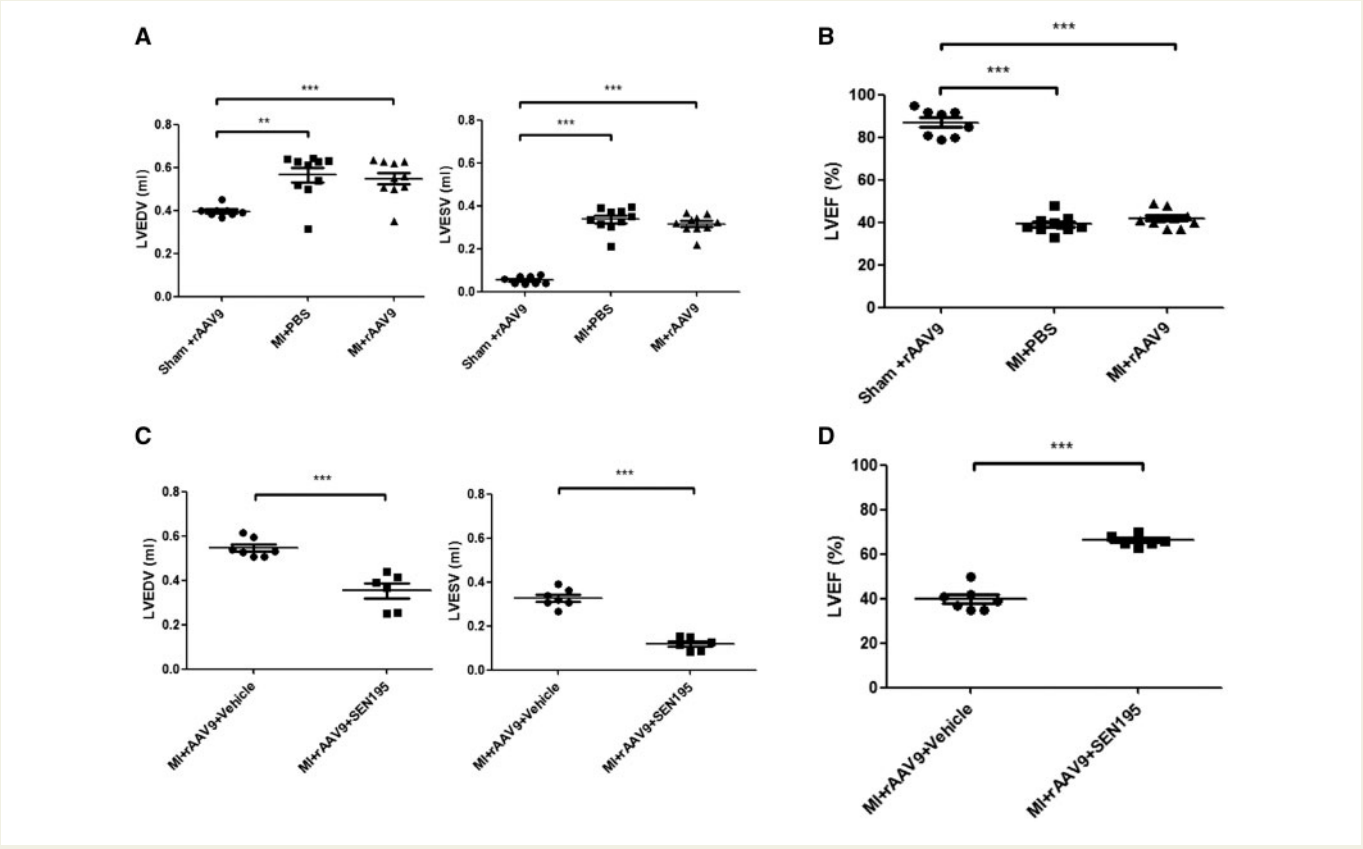

Figure 4 Cardiac function of infarcted hearts depend on the canonical Wnt/β-catenin/TCF pathway activation. Cardiac function evaluated by 1.5 T MRI. Infarcted hearts that received PBS (MI + PBS; $n = 10$) and rAAV9 (MI + rAAV9; $n = 11$) had similar progressive enlargement of LV end-diastolic (EDV, mL) and end-systolic (ESV, mL) volume (*A*; one-way ANOVA followed by Bonferroni *post hoc* test) and fall of ejection fraction (LVEF, %) (*B*; one-way ANOVA followed by Bonferroni *post hoc* test). Transduced infarcted rats that received long-term treatment with SEN195 (MI + rAAV9 + SEN195, $n = 6$) displayed a better preserved LV ESV, EDV (*C*; independent Student's *t*-test) and LVEF (*D*; independent Student's *t*-test) compared with untreated animals (MI + rAAV9 + Vehicle, $n = 7$). SHAM + rAAV9 animals ($n = 8$) were used as control. $^{**}P < 0.01$; $^{***}P < 0.001$.

3.2 Canonical Wnt signalling activity detected by MRI

Infarcted hearts receiving PBS (MI + PBS) did not display iron accumulations (*Figure 2A*). As shown in *Figure 2B*, the levels of T2* time were significantly lower in the LV border zone compared with the remote zone of infarcted transduced hearts (MI + rAAV9) (*Figure 2C*). This demonstrates the presence of iron accumulation within the LV wall, as highlighted in *Figure 2* and Supplementary material online, *Figure S1*. The mean value of LV T2* time in SHAM + rAAV9 rats was 33 ± 5 ms, indicating the absence of myocardial iron accumulation.

At 4 weeks after treatment with SEN195 (*Figure 3A and B*), the T2* time values in the border zone of infarcted transduced hearts (MI + rAAV9 + SEN195) were higher than those measured in the border zone of infarcted animals treated with Vehicle (MI + rAAV9+ Vehicle) (*Figure 3C*). The presence of iron accumulation was detected within the LV wall, as highlighted in *Figure 3* and Supplementary material online, *Figure S2*.

3.3 MRI morphological and functional assessment

As shown in *Figure 4A and B*, the LV end-systolic and end-diastolic volume, and ejection fraction of infarcted hearts were similar in MI + rAAV9 and MI + PBS groups. SEN195 significantly limited the enlargement of LV end-diastolic volume and the fall in LV ejection fraction, compared with rats treated with vehicle (*Figure 4C and D*). Heart rate was similar with all treatments (not shown).

3.4 Histological analysis of iron accumulation, immunofluorescence-detected colocalizations, and post-infarct LV remodelling

Perls-positive staining was detected in the border zone of the MI + rAAV9 group at 4 weeks after delivery of viral vectors (*Figure 5A*), but not in the MI + PBS (*Figure 5B*), and no iron load was detected in the remote zone. SHAM + rAAV9 did not show any Perls-positive cells (data not shown). As shown in *Figure 5C*, Perls-positive cells were not detectable in any LV region of transduced infarcted rodent hearts treated with SEN195. Conversely, the administration of vehicle did not affect the iron accumulation in cardiac cells of LV regions bordering the infarct scar (*Figure 5D*).

As shown in *Figure 6*, GFP positive staining was detected in Perls-positive cells in the LV border zone of MI + rAAV9 group, whereas iron was undetectable in cardiac GFP-positive cells of SHAM + rAAV9 hearts. Conversely, the colocalization of iron and GFP signals identified in LV border zone of rats treated with Vehicle was undetectable in infarcted rats after 4 weeks of treatment with SEN195, indicating that the iron load into the transduced

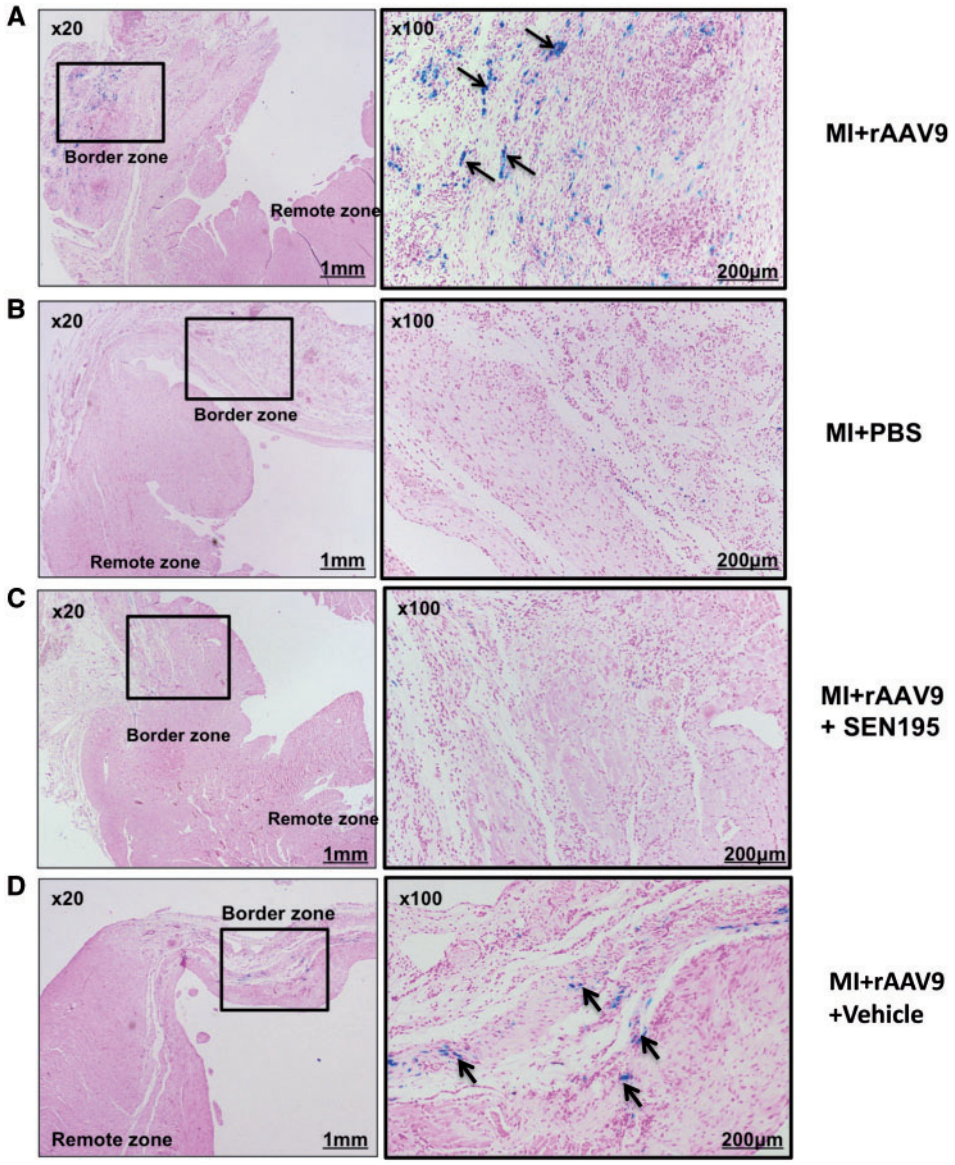

Figure 5 Iron deposition in cardiac cells of rAAV9-transduced infarcted hearts depends on the canonical Wnt/β-catenin/TCF pathway activation. Prussian Blue staining of LV tissue sections showing iron accumulation (arrows) in the infarct border zone, i.e. the site of injection of rAAV9. Iron accumulation in MI + rAAV9 (*A*) ($n = 11$) and MI + rAAV9 + Vehicle (*D*) ($n = 7$) at 4 weeks after intramyocardial injection of rAAV9. No staining was observed in the non-transduced infarcted hearts treated with PBS (*B*) ($n = 5$) or with SEN195 (*C*) ($n = 6$).

cardiac cells was related to the activity of canonical Wnt pathway. GFP was colocalized with α-SA in all transduced hearts, confirming that rAAV9 has a tropism for cardiomyocytes in accord to previous reports.[26,33] Conversely, we could not detect any association between GFP and vWF or α-SMA or NeuN positivity (see Supplementary material online, *Figure S3*). As shown in Supplementary material online, *Figure S4*, iron was detected in GFP/α-SA-positive cells in the LV border zone of transduced infarcted hearts not treated with SEN195.

Morphometric analysis of Masson's trichromic-stained LV sections showed that the anterior wall of untreated infarcted hearts underwent significant remodelling (*Figure 7A*) and the infarct scar size (% of the left ventricle) was similar in MI + PBS and MI + rAAV9 rats (*Figure 7B*). In contrast, the long-term treatment with SEN195 protected the heart against ischaemic injury compared with rats treated with Vehicle, as indicated by a significant reduction of the infarct scar size (*Figure 7C and D*).

As expected, the arteriolar density tended to increase, although not significantly ($P = 0.054$) in LV border zone compared with LV remote zone of infarcted hearts (*Figure 7G*). The long-term treatment with SEN195 significantly enhanced the number of arterioles in the LV border zone compared with rats treated with Vehicle, yet it did not affect myocardial arteriolar density in the LV remote zone (*Figure 7H*).

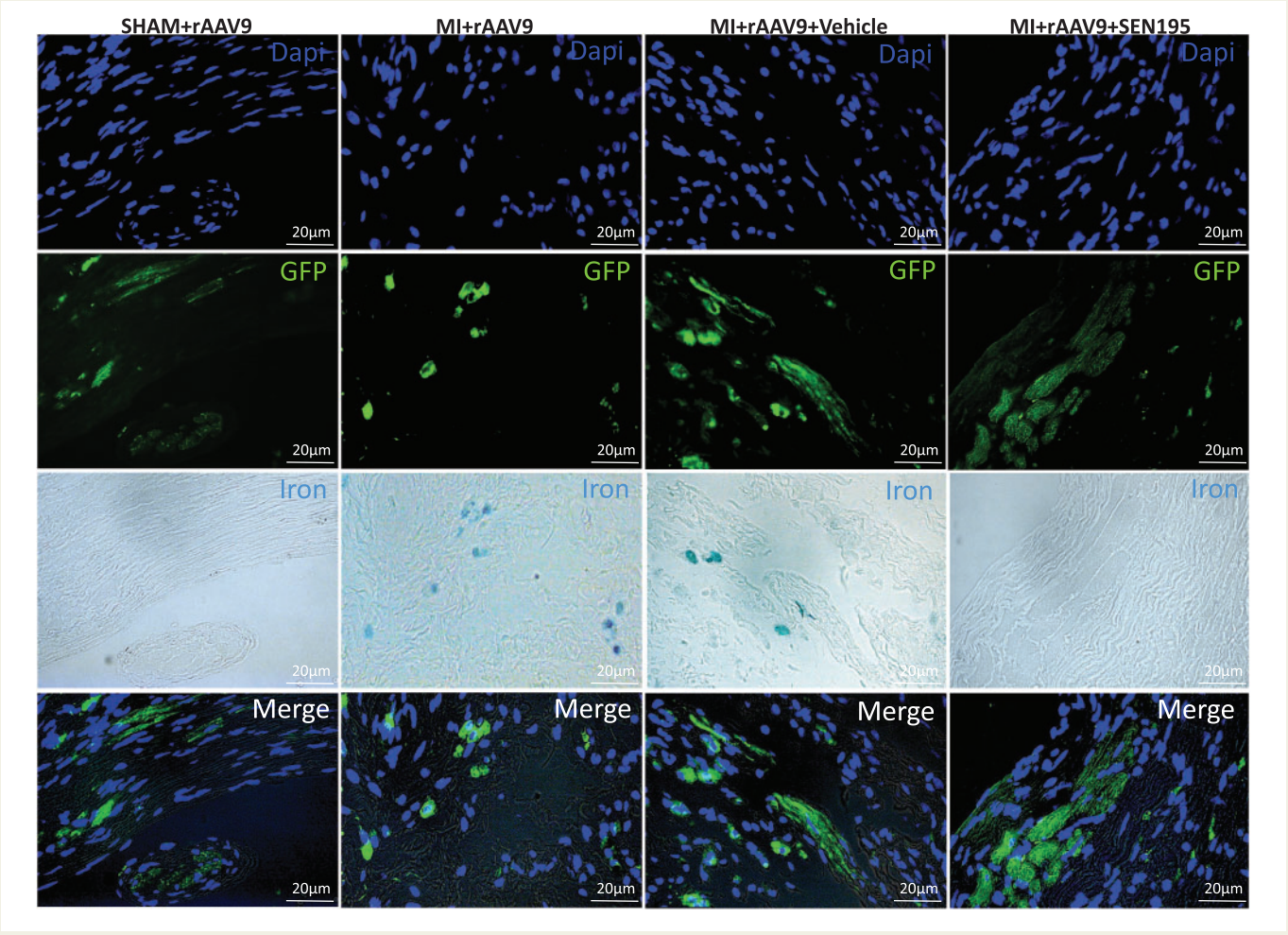

Figure 6 Iron deposition is localized in LV GFP-positive cardiac cells. Immunofluorescence co-staining of representative LV sections at 4 weeks after intramyocardial injection of rAAV9. Immunofluorescence for GFP was used for the detection of transduced cardiac cells. In the LV border zone of MI + rAAV9 ($n = 11$) and MI + rAAV9 + Vehicle hearts ($n = 7$), GFP positive cells display also iron accumulation (Perls-positive cells). Conversely, iron was undetectable in normal hearts and in infarcted hearts treated with SEN195 ($n = 6$).

4. Discussion

The present results demonstrate that the canonical Wnt/β-catenin/TCF pathway activation after acute MI can be detected, *in vivo*, by hFTH-based reporter gene MRI. The activation of TCF/Lef promoter induced the expression of hFTH and consequent regional iron accumulation in the infarct border zone, which was detected with a clinical standard 1.5 T MRI scanner and then confirmed *ex vivo* by histological analysis. On the other hand, the TCF-hFTH-BGH-PGK-copGFP dual-reporter gene proved valuable in determining whether AAV-mediated gene transfer was equally efficient in control and infarcted hearts. GFP gene, placed under the control of a constitutively active promoter, was similarly expressed in all hearts injected with AAV vectors, with and without infarction, thus indicating that (i) the reporter gene transfer was not affected by cardiac injury and (ii) iron accumulation did not interfere with the viability of transduced cells. Prussian Blue staining indicated that iron deposits were located in morphologically normal GFP-positive cells, whereas it was undetectable in GFP-negative cells and in the interstitial space of the infarcted areas. In fact, significant extracellular iron deposition is more typical of haemorrhagic reperfused myocardial infarcts[34] and it is undetectable[6,35] or rarely detectable in chronic non-reperfused infarction,[35] which is the pathological condition reproduced by our rat model.

The specificity of the TCF/Lef promoter-hFTH response to the canonical Wnt/β-catenin activation was confirmed by the absence of iron-related MRI signal in rats receiving SEN195, a small-molecule inhibitor of the poly-ADP-ribosylating (PARP) enzyme tankyrase that causes selective silencing of TCF-mediated gene transcription by promoting beta-catenin phosphorylation and degradation.[32] We have previously developed and validated 'SEN' molecules for oncological applications.[19–21] Interestingly, we found that the pharmacological inhibition of the canonical Wnt/β-catenin/TCF pathway is very beneficial for post-infarct cardiac remodelling, as shown by the notable preservation of ventricular morphology and function. Although the arteriolar density in the infarct border zone of untreated infarcted rats was significantly higher than in remote regions, it was further increased by SEN195 treatment. Our findings suggest that switching off the TCF promoter enhances the angiogenic response of infarcted myocardium, which is impaired by

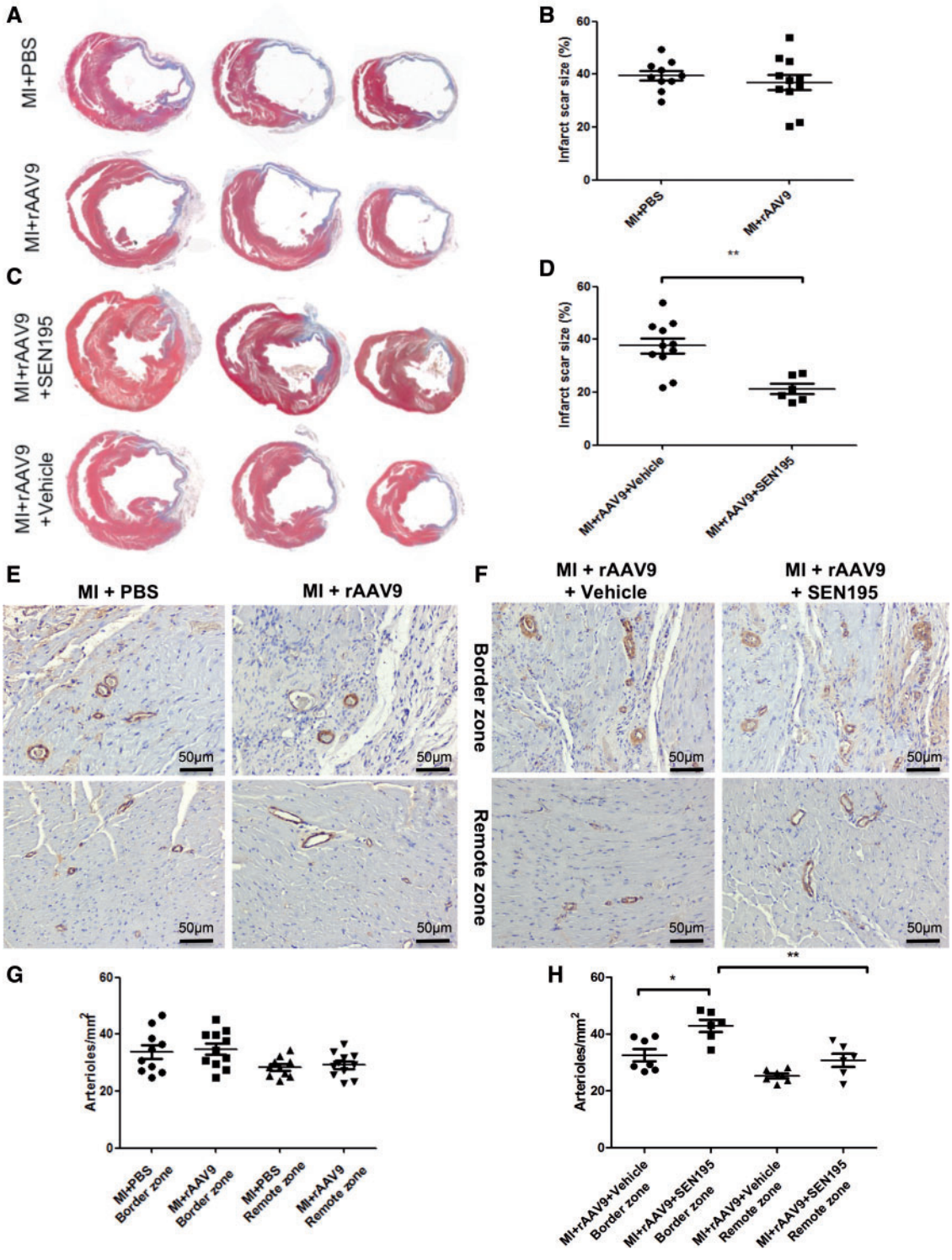

Figure 7 Structural alterations of infarcted hearts depend on the canonical Wnt/β-catenin/TCF pathway activation. Histological analysis of infarcted hearts at 4 weeks after MI. (*A–C*) Representative Masson's trichrome staining of LV transverse sections of infarcted hearts injected with PBS (MI + PBS; $n = 10$) or injected with rAAV9 (MI + rAAV9; $n = 11$) and then administered Vehicle (MI + rAAV9 + Vehicle; $n = 10$) or SEN195 (MI + rAAV9 + SEN195; $n = 6$). In the same experimental group: (*B–D*) quantification of LV infarct scar size (independent Student's *t*-test); (*E, F*) Visualization of arterioles by immunohistochemistry in the LV border and remote zone (brown, α-SMA-positive cells). (*G, H*) Quantification of arteriolar density (MI + rAAV9 + Vehicle; $n = 7$; two-way ANOVA followed by Bonferroni *post hoc* test). Values are expressed as means ± SEM. *$P < 0{,}05$; **$P < 0.01$.

ischaemic microenvironment.[36] It is known that the activation of canonical Wnt signalling by oxidative stress causes endothelial dysfunction,[37] which hampers the post-ischaemic angiogenesis[38] and promotes negative myocardial remodelling processes in humans[39] and in animal models[6,26–30,40] of post-ischaemic heart failure. These results provide further evidence that the canonical Wnt/β-catenin pathway activation exerts a negative impact on post-infarct cardiac remodelling.

Other authors have determined the Wnt/β-catenin pathway activation state using standard reporter genes identifiable only by histological analysis, *ex vivo*, and by methods, such as optical imaging, that cannot assess organ function *in vivo*.[15,9] A clear advantage of the approach utilized in our study is the possibility to non-invasively detect molecular changes, *in vivo*, while simultaneously assessing cardiac chambers with the gold standard imaging technology for quantitative measurements of morphology and function.[41] In particular, it may prove helpful for non-invasive characterization of phenotypic changes in selected cardiac regions during activation or inhibition of canonical Wnt pathway in response to various stimuli or aging. Moreover, our reporter gene technology will possibly be a tool to assess the efficacy of new Wnt inhibitors/activators in modulating myocardial remodelling at different stages, as well as to evaluate the effects of pro-regenerative therapies on the canonical Wnt pathway activity, even in large animal models. We have previously shown that the hFTH MRI reporter gene is similarly valuable for *in vivo* tracking of stem cells implanted in infarcted rat hearts.[6]

4.1 Limitations

In this study, for the first time, we provided the proof of concept that a molecular probe constituted by hFTH gene under the control of a β-catenin-responsive promoter can be utilized for MRI detection of the canonical Wnt/β-catenin pathway activation or repression. Further work will be necessary to test the reliability of this methodology for tracking changes over the entire evolution of post-infarct remodelling or under other physiological and pathological conditions. Secondly, we utilized SEN195, a tankyrase inhibitor, to verify whether the hFTH reporter gene signal could be muted when Wnt/β-catenin pathway activation was blocked after infarction. By doing so, we could also document a marked beneficial effect of SEN195 administration; however, specifically designed studies will be necessary to deeply characterize the therapeutic actions of this β-catenin inhibitor on infarcted hearts.

5. Conclusions

We developed a novel TCF/Lef promoter-hFTH construct that displays satisfactory MRI reporter gene properties for *in vivo* detection of the canonical Wnt/β-catenin/TCF activation state in response to cardiac injury and therapeutic interventions. This technology, based on clinical standard MRI and adaptable to other pathways by varying the specific promoter, can potentially prove a powerful tool for the combined, non-invasive evaluation of molecular and morpho-functional alterations characterizing many cardiac pathophysiological conditions.

Supplementary material

Supplementary material is available at *Cardiovascular Research* online.

Acknowledgement

We would like to thank Gaia Papini for her helpful technical support.

Conflict of interest: none declared.

Funding

This work was supported by grant from Regione Toscana POR CReO cofounded by European Regional Development Fund for Regional Competitiveness and Employment Objectives, 2007-2013 and by R01 HL-108213 (NIH).

References

1. Genove G, DeMarco U, Xu H, Goins WF, Ahrens ET. A new transgene reporter for in vivo magnetic resonance imaging. *Nat Med* 2005;**11**:450–454.
2. Cohen B, Ziv K, Plaks V, Israely T, Kalchenko V, Harmelin A, Benjamin LE, Neeman M. MRI detection of transcriptional regulation of gene expression in transgenic mice. *Nat Med* 2007;**13**:498–503.
3. Kim HS, Cho HR, Choi SH, Woo JS, Moon WK. In vivo imaging of tumor transduced with bimodal lentiviral vector encoding human ferritin and green fluorescent protein on a 1.5T clinical magnetic resonance scanner. *Cancer Res* 2010;**70**:7315–7324.
4. Iordanova B, Goins WF, Clawson DS, Hitchens TK, Ahrens ET. Quantification of HSV-1-mediated expression of the ferritin MRI reporter in the mouse brain. *Gene Ther* 2013;**20**:589–96.
5. Kim HS, Woo J, Choi Y, Hwang EH, Choi SK, Cho KW, Moon WK. Noninvasive MRI and multilineage differentiation capability of ferritin-transduced human mesenchymal stem cells. *NMR Biomed* 2015;**28**:168–179.
6. Campan M, Lionetti V, Aquaro GD, Forini F, Matteucci M, Vannucci L, Chiuppesi F, Di Cristofano C, Faggioni M, Maioli M, Barile L, Messina E, Lombardi M,Pucci A, Pistello M, Recchia FA. Ferritin as a reporter gene for in vivo tracking of stem cells by 1.5-T cardiac MRI in a rat model of myocardial infarction. *Am J Physiol Heart Circ Physiol* 2011;**300**:H2238–2250.
7. Kim HS, Joo HJ, Woo JS, Choi YS, Choi SH, Kim H, Moon WK. In vivo magnetic resonance imaging of transgenic mice expressing human ferritin. *Mol Imaging Biol* 2013;**15**: 48–57.
8. Dawson K, Aflaki M, Nattel S. Role of the Wnt-Frizzled system in cardiac pathophysiology: a rapidly developing, poorly understood area with enormous potential. *J Physiol* 2013;**591**:1409–1432.
9. Barolo S. Transgenic Wnt/TCF pathway reporters: all you need is Lef? *Oncogene* 2006;**25**:7505–7511.
10. Wöhrle S, Wallmen B, Hecht A. Differential control of Wnt target genes involves epigenetic mechanisms and selective promoter occupancy by T-cell factors. *Mol Cell Biol* 2007;**27**:8164–8177.
11. Zelarayán LC, Noack C, Sekkali B, Kmecova J, Gehrke C, Renger A, Zafiriou MP, van der Nagel R, Dietz R, de Windt LJ, Balligand JL, Bergmann MW. Beta-Catenin downregulation attenuates ischemic cardiac remodeling through enhanced resident precursor cell differentiation. *Proc Natl Acad Sci USA* 2008;**105**:19762–19767.
12. Sklepkiewicz P, Shiomi T, Kaur R, Sun J, Kwon S, Mercer B, Bodine P, Schermuly RT, George I, Schulze PC, D'Armiento JM. Loss of secreted frizzled-related protein-1 leads to deterioration of cardiac function in mice and plays a role in human cardiomyopathy. *Circ Heart Fail* 2015;**8**:362–372.
13. Baurand A, Zelarayan L, Betney R, Gehrke C, Dunger S, Noack C, Busjahn A, Huelsken J, Taketo MM, Birchmeier W, Dietz R, Bergmann MW. Beta-catenin downregulation is required for adaptive cardiac remodeling. *Circ Res* 2007;**100**:1353–1362.
14. Zhao X, Hua Y, Chen H, Yang H, Zhang T, Huang G, Fan H, Tan Z, Huang X, Liu B, Zhou Y. Aldehyde dehydrogenase-2 protects against myocardial infarction-related cardiac fibrosis through modulation of the Wnt/β-catenin signaling pathway. *Ther Clin Risk Manag* 2015;**11**:1371–1381.
15. Oerlemans MI, Goumans MJ, van Middelaar B, Clevers H, Doevendans PA, Sluijter JP. Active Wnt signaling in response to cardiac injury. *Basic Res Cardiol* 2010;**105**:631–641.
16. Thirunavukkarasu M, Han Z, Zhan L, Penumathsa SV, Menon VP, Maulik N. Adeno-sh-beta-catenin abolishes ischemic preconditioning-mediated cardioprotection by downregulation of its target genes VEGF, Bcl-2, and survivin in ischemic rat myocardium. *Antioxid Redox Signal* 2008;**10**:1475–1484.
17. Duan J, Gherghe C, Liu D, Hamlett E, Srikantha L, Rodgers L, Regan JN, Rojas M, Willis M, Leask A, Majesky M, Deb A. Wnt1/βcatenin injury response activates the epicardium and cardiac fibroblasts to promote cardiac repair. *EMBO J* 2012;**31**:429–442.
18. Hahn JY, Cho HJ, Bae JW, Yuk HS, Kim KI, Park KW, Koo BK, Chae IH, Shin CS, Oh BH, Choi YS, Park YB, Kim HS. Beta-catenin overexpression reduces myocardial infarct size through differential effects on cardiomyocytes and cardiac fibroblasts. *J Biol Chem* 2006;**281**:30979–30989.

19. Nencini A, Pratelli C, Quinn JM, Salerno M, Tunici P, De Robertis A, Valensin S, Mennillo F, Rossi M, Bakker A, Benicchi T, Cappelli F, Turlizzi E, Nibbio M, Caradonna NP, Zanelli U, Andreini M, Magnani M, Varrone M. Structure-activity relationship and properties optimization of a series of quinazoline-2,4-diones as inhibitors of the canonical Wnt pathway. *Eur J Med Chem* 2015;**95**:526–545.
20. De Robertis A, Valensin S, Rossi M, Tunici P, Verani M, De Rosa A, Giordano C, Varrone M, Nencini A, Pratelli C, Benicchi T, Bakker A, Hill J, Sangthongpitag K, Pendharkar V, Liu B, Ng FM, Then SW, Jing Tai S, Cheong SM, He X, Caricasole A, Salerno M. Identification and characterization of a small-molecule inhibitor of Wnt signaling in glioblastoma cells. *Mol Cancer Ther* 2013;**12**:1180–1189.
21. De Robertis A, Mennillo F, Rossi M, Valensin S, Tunici P, Mori E, Caradonna N, Varrone M, Salerno M. Human sarcoma growth is sensitive to small-molecule mediated AXIN stabilization. *PLoS One* 2014;**9**:e97847.
22. Shibamoto S, Higano K, Takada R, Ito F, Takeichi M, Takada S. Cytoskeletal reorganization by soluble Wnt3a protein signalling. *Genes Cells* 1998;**3**:659–670.
23. Vandesompele J, De Preter K, Pattyn F, Poppe B, Van Roy N, De Paepe A, Speleman F. Accurate normalization of real-time quantitative RT-PCR data by geometric averaging of multiple internal control genes. *Genome Biol* 2002;**3**:RESEARCH0034.
24. Cohen ED, Miller MF, Wang Z, Moon RT, Morrisey EE. Wnt5a and Wnt11 are essential for second heart field progenitor development. *Development* 2012;**139**:1931–1940.
25. Gujral TS, MacBeath GA, Isalan M, ed. System-wide investigation of the dynamics of wnt signaling reveals novel phases of transcriptional regulation. *PLoS One*; 2010;**5**:e10024.
26. Zentilin L, Puligadda U, Lionetti V, Zacchigna S, Collesi C, Pattarini L, Ruozi G, Camporesi S, Sinagra G, Pepe M, Recchia FA, Giacca M. Cardiomyocyte VEGFR-1 activation by VEGF-B induces compensatory hypertrophy and preserves cardiac function after myocardial infarction. *FASEB J* 2010;**24**:1467–1478.
27. Lionetti V, Cantoni S, Cavallini C, Bianchi F, Valente S, Frascari I, Olivi E, Aquaro GD, Bonavita F, Scarlata I, Maioli M, Vaccari V, Tassinari R, Bartoli A,Recchia FA, Pasquinelli G, Ventura C. Hyaluronan mixed esters of butyric and retinoic acid affording myocardial survival and repair without stem cell transplantation. *J Biol Chem* 2010;**285**:9949–9961.
28. Forini F, Lionetti V, Ardehali H, Pucci A, Cecchetti F, Ghanefar M, Nicolini G, Ichikawa Y, Nannipieri M, Recchia FA, Iervasi G. Early long-term L-T3 replacement rescues mitochondria and prevents ischemic cardiac remodelling in rats. *J Cell Mol Med* 2011;**15**:514–524.
29. Ventura C, Cantoni S, Bianchi F, Lionetti V, Cavallini C, Scarlata I, Foroni L, Maioli M, Bonsi L, Alviano F, Fossati V, Bagnara GP, Pasquinelli G, Recchia FA, Perbellini A. Hyaluronan mixed esters of butyric and retinoic Acid drive cardiac and endothelial fate in term placenta human mesenchymal stem cells and enhance cardiac repair in infarcted rat hearts. *J Biol Chem* 2007;**282**:14243–14252.
30. Barile L, Lionetti V, Cervio E, Matteucci M, Gherghiceanu M, Popescu LM, Torre T, Siclari F, Moccetti T, Vassalli G. Extracellular vesicles from human cardiac progenitor cells inhibit cardiomyocyte apoptosis and improve cardiac function after myocardial infarction. *Cardiovasc Res* 2014;**103**:530–541.
31. Westwood M, Anderson LJ, Firmin DN, Gatehouse PD, Charrier CC, Wonke B, Pennell DJ. A single breath-hold multiecho T2* cardiovascular magnetic resonance technique for diagnosis of myocardial iron overload. *J Magn Reson Imaging* 2003;**18**:33–39.
32. Huang SM, Mishina YM, Liu S, Cheung A, Stegmeier F, Michaud GA, Charlat O, Wiellette E, Zhang Y, Wiessner S, Hild M, Shi X, Wilson CJ, Mickanin C, Myer V, Fazal A, Tomlinson R, Serluca F, Shao W, Cheng H, Shultz M, Rau C, Schirle M, Schlegl J, Ghidelli S, Fawell S, Lu C, Curtis D, Kirschner MW, Lengauer C, Finan PM, Tallarico JA, Bouwmeester T, Porter JA, Bauer A, Cong F. Tankyrase inhibition stabilizes axin and antagonizes Wnt signalling. *Nature* 2009;**461**:614–620.
33. Qi Y, Liu X, Li H, Shenoy V, Li Q, Hauswirth WW, Sumners C, Katovich MJ. Selective tropism of the recombinant adeno-associated virus 9 serotype for rat cardiac tissue. *J Gene Med* 2010;**12**:22–34.
34. Kali A, Kumar A, Cokic I, Tang RL, Tsaftaris SA, Friedrich MG, Dharmakumar R. Chronic manifestation of postreperfusion intramyocardial hemorrhage as regional iron deposition: a cardiovascular magnetic resonance study with ex vivo validation. *Circ Cardiovasc Imaging* 2013;**6**:218–228.
35. Cokic I, Kali A, Wang X, Yang HJ, Tang RL, Thajudeen A, Shehata M, Amorn AM, Liu E, Stewart B, Bennett N, Harlev D, Tsaftaris SA, Jackman WM, Chugh SS, Dharmakumar R. Iron deposition following chronic myocardial infarction as a substrate for cardiac electrical anomalies: initial findings in a canine model. *PLoS One* 2013;**8**:e73193.
36. Vikram A, Kim YR, Kumar S, Naqvi A, Hoffman TA, Kumar A, Miller FJ Jr, Kim CS, Irani K. Canonical Wnt signaling induces vascular endothelial dysfunction via p66Shc-regulated reactive oxygen species. *Arterioscler Thromb Vasc Biol* 2014;**34**:2301–2309.
37. Maulik N, Das DK. Potentiation of angiogenic response by ischemic and hypoxic preconditioning of the heart. *J Cell Mol Med* 2002;**6**:13–24.
38. Most P, Lerchenmuller C, Rengo G, Mahlmann A, Ritterhoff J, Rohde D, Goodman C, Busch CJ, Laube F, Heissenberg J, Pleger ST, Weiss N, Katus HA, Koch WJ, Peppel K. S100A1 deficiency impairs postischemic angiogenesis via compromised proangiogenic endothelial cell function and nitric oxide synthase regulation. *Circ Res* 2013;**112**:66–78.
39. Lionetti V, Matteucci M, Ribezzo M, Di Silvestre D, Brambilla F, Agostini S, Mauri P, Padeletti L, Pingitore A, Delsedime L, Rinaldi M, Recchia FA, Pucci A. Regional mapping of myocardial hibernation phenotype in idiopathic end-stage dilated cardiomyopathy. *J Cell Mol Med* 2014;**18**:396–414.
40. Simioniuc A, Campan M, Lionetti V, Marinelli M, Aquaro GD, Cavallini C, Valente S, Di Silvestre D, Cantoni S, Bernini F, Simi C, Pardini S, Mauri P, Neglia D, Ventura C, Pasquinelli G, Recchia FA. Placental stem cells pre-treated with a hyaluronan mixed ester of butyric and retinoic acid to cure infarcted pig hearts: a multimodal study. *Cardiovasc Res* 2011;**90**:546–556.
41. Pennell DJ. Cardiovascular magnetic resonance. *Circulation* 2010;**121**:692–705.